energy&fuels

Article

pubs.acs.org/EF

Asphaltene Deposition in Different Depositing Environments: Part 1. Model Oil

Mohammad Tavakkoli,[†,‡,§] Sai R. Panuganti,[†,‡] Francisco M. Vargas,[‡] Vahid Taghikhani,[§] Mahmoud Reza Pishvaie,[§] and Walter G. Chapman*[,‡]

[‡]Department of Chemical and Biomolecular Engineering, Rice University, Houston, Texas 77005, United States

[§]Department of Chemical and Petroleum Engineering, Sharif University of Technology, Tehran, Iran

ABSTRACT: Among the asphaltene flow assurance issues, the most major concern because of asphaltene is its potential to deposit in reservoir, well tubing, flow lines, separators, and other systems along production lines causing significant production losses. Hence, the focus of this study is to understand the depositional tendency of asphaltene using quartz crystal microbalance with dissipation (QCM−D) measurements. The results are presented in two consecutive papers, with this paper (part 1) dealing with model oil systems. The depositing environment is varied by changing the system temperature, asphaltene polydispersity, solvent (asphaltene stability), depositing surface, and flow rate. This paper also discusses the roles of convective, diffusive, and adsorption kinetics on asphaltene deposition by modeling the adsorbed mass before asphaltene precipitation onset. The successive paper (part 2; 10.1021/ef401868d) will deal with real crude oil systems and modeling of the deposited mass after asphaltene precipitation onset.

1. INTRODUCTION

Asphaltene is a solubility class of compounds present in crude oil. Knowledge on the deposition mechanism of asphaltene and the factors influencing it are important in many different domains of the oil industry, for example, alteration of reservoir rock wettability because of adsorption of asphaltene,[1] plugging of flow lines because of asphaltene deposit buildup,[2] and refinery catalyst deactivation because of asphaltene adsorption at active sites.[3] Accordingly, appropriate mitigation techniques, such as a suitable surfactant-coating material for surfaces exposed to asphaltene or operating conditions, can be identified.

Quartz crystal microbalance with dissipation (QCM−D) experiments are performed here to study different depositional aspects of asphaltene from model oil (part 1) and real crude oil (part 2; 10.1021/ef401868d) systems. The QCM is a highly sensitive equipment for detecting the adsorption of a species and has been extensively used in the fields of biomaterials, cell and molecular biology, cellulose, polymers, lipids, pharmaceuticals, proteins, environment, and nanoparticles.[4−12] Few researchers have also used a QCM for investigating asphaltene adsorption kinetics.

Ekholm et al. used QCM−D to investigate the adsorption of asphaltene and resin on a gold surface.[13] Their results showed that, unlike resin, asphaltenes are irreversibly adsorbed in multilayers from toluene and heptol (50:50 *n*-heptane in toluene) solutions. Xie and Karan studied kinetics and thermodynamics of asphaltene adsorption from toluene−heptane and toluene−pentane solutions on a gold surface using a QCM in a flow-cell system.[14] The asymptotic analyses indicate an initial adsorption process controlled by the diffusion of asphaltene from bulk solution to the adsorption surface. The thermodynamic free energy predictions by Xie and Karan suggested that asphaltene would adsorb preferentially in the order of gold > stainless-steel > aluminum surfaces. More recently, Rudrake et al. used a combined QCM and X-ray photoelectron spectroscopy to investigate asphaltene−metal interactions.[15] The fractional coverage data for Cold Lake asphaltene on a gold surface followed a Langmuir (type-I) isotherm. Farooq et al. performed an interesting study for desorption of asphaltene into low-saline aqueous solutions from a saturated silica surface.[16]

Although previous researchers have investigated asphaltene adsorption on metal surfaces, what has been missing in previous studies is a model to reproduce the QCM−D experimental data in real time. There are no data on the effect of the temperature on the kinetics of asphaltene adsorption. Also, the effect of the flow rate has not been fully understood. Most of the researchers just reported the maximum amount of mass adsorbed within the experimental time scale.

The objective of this paper is to provide information on the deposition tendency of asphaltene from model oil systems in different depositing environments. To investigate the effect of the temperature, experiments at 20, 40, 60, and 80 °C are performed using a temperature-controlled chamber. To study the effect of asphaltene polydispersity, both *n*-pentane- and *n*-heptane-extracted asphaltene are used for adsorption. To observe the impact of asphaltene stability on its deposition, heptol solutions with varying heptane/toluene ratios are used as solvents. To understand the interactions between asphaltene and various surfaces, crystals coated with gold, carbon steel and iron oxide are used. The flow rate is varied by 100 orders of magnitude to check the effect of convective transfer on the

Special Issue: 14th International Conference on Petroleum Phase Behavior and Fouling

Received: September 17, 2013
Revised: November 20, 2013
Published: December 2, 2013

asphaltene adsorption process. Most importantly, a model is presented to capture the adsorption process in a QCM−D before the asphaltene precipitation onset. A novel method proposed by Vargas for the detection of asphaltene precipitation onset is used here.[17]

2. EXPERIMENTAL SECTION

For this paper, experiments are conducted to investigate the kinetics of asphaltene adsorption on different surfaces from different model oil systems at various temperatures. The following subsections describe the methods for asphaltene extraction, asphaltene model oil solution preparation, asphaltene adsorption experiments using QCM−D, atomic force microscopy (AFM), and determination of asphaltene precipitation onset. All of the reagents used are high-performance liquid chromatography (HPLC)-grade procured from Sigma-Aldrich.

2.1. Sample Preparation. *2.1.1. Asphaltene Extraction.* A crude oil (S) with a long history of asphaltene depositional problems during oil production is used for asphaltene sample extraction. The following asphaltene extraction procedure is employed for all of the asphaltene precipitating agents used in this study.

The oil sample is added to *n*-alkane in a 1:40 (vol/vol) ratio of crude oil/asphaltene precipitating agent. The mixture is prepared in a dark beaker and sonicated for 45 min using a VWR Branson Sonifier. The temperature is maintained constant during the sonification process to maintain the *n*-alkane-diluted crude oil equilibrium. The mixture is allowed to age for 2 days in a dark and cool corner of the laboratory with a 45 min sonification each day. After aging, the solution is vacuum-filtered using a 0.2 μm nylon membrane filter. The filter cake is installed in a Soxhlet apparatus. The solvent used in the round-bottomed flask of the Soxhlet apparatus is the same as the asphaltene precipitating agent, which was added to the oil sample in the first stage of extraction. The system is run at the solvent boiling temperature until the run-down effluent is colorless. The Soxhlet apparatus is allowed to cool and then run with toluene as the solvent to dissolve the now impurity-free asphaltene remaining in the filter cake. The system is continued running until the run-down effluent is colorless.

The solution of toluene with asphaltene is transferred to a beaker with a wide opening and a known weight. The beaker is then left open in an oven at 80 °C for 1 day to evaporate toluene. The amount of pure asphaltene can be obtained by knowing the weight of beaker plus asphaltene. Asphaltene extracted using *n*-pentane as the asphaltene precipitating agent is termed as *n*-C_5 asphaltene. Similarly, *n*-C_7 asphaltene is defined and used alongside *n*-C_5 asphaltene to understand the polydispersity effect on deposition.

2.1.2. Asphaltene Solution Preparation. To prepare the base asphaltene solution, 100 mL of toluene is added to the extracted asphaltene in the beaker. The mixture is stirred with a glass rod and then sonicated using a Fisher Scientific Sonication Bath (FS60) for 20 min. The mixture is allowed to equilibrate for 1 day and then filtered using a 0.2 μm Nylon filter paper to remove the undissolved asphaltene particles. After filtration, the filter paper is dried and weighed to calculate the actual mass of asphaltene in the solution. The filtered solution is transferred into a volumetric flask, and a required amount of toluene is added to make a base solution of known concentration. The base solution is stored in a dark and cool place for future use. Each time before starting the QCM−D experiment, a portion of the base solution is diluted to the required concentration for the experiment. The prepared experimental sample is sonicated for 20 min using the sonication bath and then equilibrated for 10 min before injecting into the QCM−D setup.

2.2. Asphaltene Adsorption Experiments. *2.2.1. QCM Setup.* The Q-Sense high-temperature chamber (QHTC) 101 (Q-Sense AB, Sweden) with a working temperature of 4−150 °C is used in this study. The chamber includes a Flow Module 401 made of titanium. The AT-cut sensor crystal (5 MHz) with a diameter of 14 mm is used inside the flow module. Flow lines and pump tubing are made of Teflon. The temperature- and solvent-resistant o-rings and sealing gaskets are used in this study. The instrument monitors in real time the series resonant frequency and dissipation of the freely oscillating crystal by numerically curve fitting the decay voltage to an exponentially damped sinusoidal when the power is disconnected.

2.2.2. Procedure. The system is assembled with a clean sensor crystal mounted inside the flow module. The absolute dissipation values are checked in air to make sure that the sensor crystal is rightly mounted and not damaged. Then, the asphaltene-free solvent is injected into the system using a peristaltic pump. Liquid is introduced through tubing with a 0.75 mm internal diameter. The residence time is around 7 min for the liquid before reaching the sensor crystal. The system is left to stabilize in the solvent to establish a baseline of the measurement. The system is considered stable if the changes in the frequencies are less than 1 Hz in 20 min. Then, the main solution, asphaltene plus solvent, is injected at a constant flow rate. To ensure a homogeneous oil−asphaltene slurry system, samples beyond the onset of asphaltene precipitation are continuously sonicated prior to injection. The instrument records frequencies and dissipations at different harmonics for the sensor crystal. Then, the data are processed with QTools software from Q-Sense.

2.2.3. Cleaning Procedure. A chemical treatment procedure is used to remove the asphaltene particles from the gold crystal surface. After the experiment, the sensor crystal is placed in a crystal holder and sonicated in toluene using a sonication bath for 20 min. Then, it is left in hot toluene for 0.5 h. After that, the sensor crystal is dried with nitrogen and put through an ultraviolet (UV) light ozone chamber for about 1 h. After UV light, it is placed in a crystal holder and immersed in a heated cleaning solution for 20 min. The cleaning solution consists of a 5:1:1 volume ratio mixture of deionized water, ammonium hydroxide, and hydrogen peroxide heated to a temperature of 75 °C. After 20 min, the sensor crystal is rinsed with deionized water 3 times and then dried with nitrogen gas. The dried sensor crystal is placed once again under the UV lamp for UV ozone treatment for about 1 h. In this procedure, we increased the duration of each step in comparison to the cleaning procedure used by other researchers,[15,18] because our asphaltene particles were very sticky and could not be easily removed using the standard procedure for gold crystal surface cleaning.

For the carbon steel sensor, UV ozone treatment could not be used because it would break the carbon bond on the crystal surface. Therefore, after sonicating the crystal in toluene for 20 min and drying under nitrogen, a 2 wt % Hellmanex III solution for 40 min at 35 °C is used. Then, the sensor crystal is rinsed with deionized water 3 times and dried under nitrogen gas. The same cleaning procedure used for carbon steel crystal is also applied for the iron oxide sensor.

To make sure that the sensor crystal surface is clean using the above procedures, response of the sensor to 1 wt % sodium dodecyl sulfate in deionized water is measured before first use and after the cleaning procedure (after the experiment). Using the proposed procedures, responses of the sensor to sodium dodecyl sulfate solution are very close before and after surface cleaning. The life span of each sensor crystal is 4−5 experimental runs.

The flow module is also cleaned after each test. The module is flushed with toluene, dried in air, and then cleaned with 1 wt % sodium dodecyl sulfate in deionized water. Finally, the module is rinsed with deionized water and dried with nitrogen gas.

2.3. Sample Analysis. *2.3.1. Asphaltene Precipitation Onset Measurement.* The establishment and details of the procedure can be found elsewhere.[19] The working mechanism is only briefly reviewed here for our specific case of *n*-heptane/toluene−asphaltene mixtures. Test tubes containing asphaltene model oils with different ratios of *n*-heptane and toluene are prepared, starting from pure toluene, 1:9 (10 vol % heptane), 2:8, etc. The test tubes are shaken vigorously by hand and allowed to stand undisturbed for 1 h. Then, the test tubes are centrifuged at 5000 rpm for 10 min in an Eppendorf centrifuge 5804. A total of 1 mL of the supernatant liquid is taken and diluted with 4 mL of toluene. Then, the absorbance at an UV−vis wavelength of 500 nm is measured, using toluene as the blank. Finally, the values of absorbance as a function of the volume fraction of heptane are plotted. The sudden deviation in the data points corresponds to the volume fraction of *n*-heptane at the precipitation onset.

dx.doi.org/10.1021/ef401857t | Energy Fuels 2014, 28, 1617−1628

The working principle behind the proposed procedure is that, when asphaltenes are unstable even to the slightest extent in the oil system, they are removed by centrifugation and the optical density of the remaining liquid changes. Thus, precipitation independent of aggregation is measured in the current asphaltene onset determination procedure. Previous researchers used direct methods, such as the gravimetric technique, filtration experiments, microscopy, and near infrared (NIR), to determine the asphaltene precipitation onset. Such methods require a minimum asphaltene particle size to be detected. Thus, precipitation followed by aggregation is involved, and one can find various precipitation onsets at different aging times in direct methods.

On the basis of the results obtained from the proposed indirect method, it is observed that changing the aging time has no effect on the final result for precipitation onset. In other words, pure onset of asphaltene precipitation is obtained without considering aggregation effects. Figures 1 and 2 show the results of the proposed onset

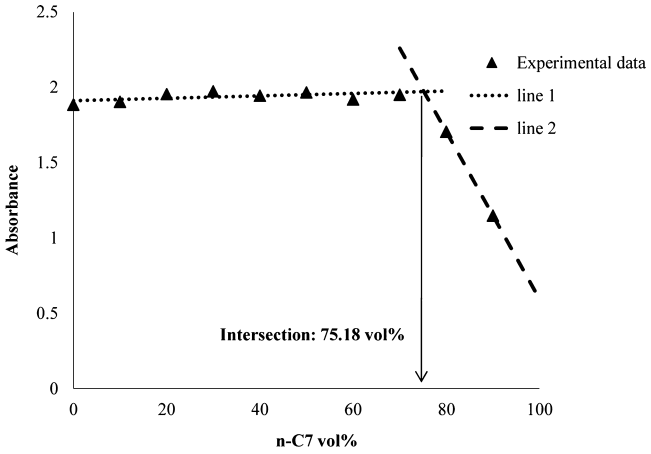

Figure 1. Precipitation onset measurement for a 1 h aged sample. The absorbance of UV−vis is 500 nm wavelength.

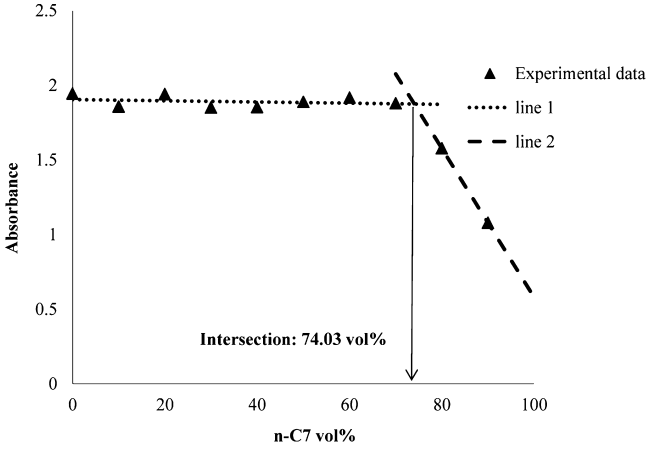

Figure 2. Precipitation onset measurement for a 24 h aged sample. The absorbance of UV−vis is 500 nm wavelength.

determination method at 500 nm wavelength and at aging time of 1 and 24 h, respectively. The sample consists of 10 vol % crude oil (S) and 90 vol % heptol. For this system, the determined precipitation onset is 75.18 and 74.03 vol % *n*-heptane for aging times of 1 and 24 h, respectively, which shows the independence of asphaltene precipitation onset to the aging time.

2.3.2. AFM. Images of the asphaltene-deposited sensor crystal are captured using a NanoScope IIIA atomic force microscope. Imaging is performed in air at room temperature using tapping mode. The images are scanned at 5 × 5 μm^2. The diameter of the adsorbed species is analyzed using the NanoScope Analysis software.

3. MODELING

This section shows how the experimental results are further interpreted by modeling.

3.1. Frequency and Dissipation Changes. There can be three main contributions to the frequency and dissipation of the sensor crystals because of the adsorbed film: (a) mass loading, (b) liquid loading, and (c) liquid trapping. The equations describing each contribution are as follows:

mass loading[20]

$$\Delta f_{\text{adsorption}} - \frac{2nf_0^2}{\rho_q v_q}\frac{\Delta m}{A} = -\frac{n\Delta\Gamma}{C} \tag{1}$$

liquid loading[21,22]

$$\Delta f_{\text{liquid loading}} = -\sqrt{\frac{n}{\pi}}\frac{f_0^{3/2}}{\rho_q v_q}(\sqrt{\rho_l \eta_l} - \sqrt{\rho_s \eta_s}) \tag{2}$$

$$\Delta D_{\text{liquid loading}} = -\frac{1}{\sqrt{n\pi}}\frac{2f_0^{1/2}}{\rho_q v_q}(\sqrt{\rho_l \eta_l} - \sqrt{\rho_s \eta_s}) \tag{3}$$

liquid trapping[23]

$$\Delta f_{\text{liquid trapping}} = -\frac{2f_0^2}{\rho_q v_q}h_l(\rho_l - \rho_s) \tag{4}$$

where f_0 is the fundamental resonant frequency ($f_0 = 5 \times 10^6$ Hz), n is the overtone number ($n = f_n/f_0 = 1, 3, 5, 7, 9, 11$, and 13), Δm is the adsorbed mass, $\Delta\Gamma$ is the adsorbed mass density, A is the active area of the sensor crystal (0.785 cm^2), ρ_q is the specific density of quartz (2650 kg/m^3), v_q is the shear wave velocity in quartz (3340 m/s), $v_q = (\mu_q/\rho_q)^{1/2} = 2f_0 h_q$, μ_q is the shear modulus of quartz (2.947×10^{10} Pa), h_q is the thickness of the quartz crystal (3.37×10^{-4} m), h_l is the thickness of trapped liquid, and C is the constant of the quartz crystal (17.7 ng Hz^{-1} cm^{-2} for a 5 MHz crystal). ρ is the density, η is the viscosity, and subscripts s and l refer to the solvent and liquid mixtures, respectively.

When asphaltene particles are adsorbed onto the sensor crystal, it can be treated as an equivalent mass change of the crystal itself. An increase in mass, Δm induces a proportional shift in frequency, Δf. This linear relationship between Δm and Δf was first demonstrated by Sauerbrey in eq 1. The relationship is valid when the following conditions are fulfilled: (1) The adsorbed mass is distributed evenly over the sensor crystal. (2) Δm is much smaller than the mass of the sensor crystal itself (<1%). (3) The adsorbed mass is rigidly attached, with no slip or inelastic deformation in the added mass because of the oscillatory motion.

The last condition is valid when the frequency decreases in proportion to the true mass of the adsorbate with no change in energy dissipation, ΔD. The characteristics for a rigid film are as follows: (1) All harmonics overlay in Δf responses. (2) ΔD is small (more specifically, $\Delta D/\Delta f \ll 0.4 \times 10^{-6}$ Hz^{-1}).[24]

When a sensor crystal is operated in Newtonian liquid phase, the liquid becomes coupled to the crystal oscillation and the increase in density and/or viscosity of the medium leads to a rise in both frequency and dissipation factor.[21,22] An example of the liquid loading effect is when crude oil is introduced into

dx.doi.org/10.1021/ef401857t | *Energy Fuels* 2014, 28, 1617−1628

heptol rather than asphaltene into heptol. Additional shifts may arise with surface roughness because of liquid trapping by interfacial cavities and pores.[25,26] This contribution is usually small, and liquid trapping could be neglected using smooth surfaces.[18]

In some cases, the adsorbed film does not show a rigid behavior and the following characteristics can be seen: (1) spreading of the overtones in Δf responses and (2) ΔD being high and comparable to Δf (meaning $\Delta D/\Delta f \ll 0.4 \times 10^{-6}$ Hz^{-1} is no longer valid).

These characteristics show a viscoelastic (soft) film. In this case, the viscoelastic behavior can be characterized by measuring the resonance curves at multiple frequencies according to the Voigt model.[27] In the current asphaltene study, all experiments showed viscoelastic behavior for the adsorbed layer from the model oil system onto the sensor crystal surface. Figure 3 presents frequency and dissipation changes versus time for the adsorption of *n*-pentane asphaltene from the asphaltene + toluene system onto a gold quartz crystal surface. In Figure 3, Δf and ΔD represent an adsorbed viscoelastic film.

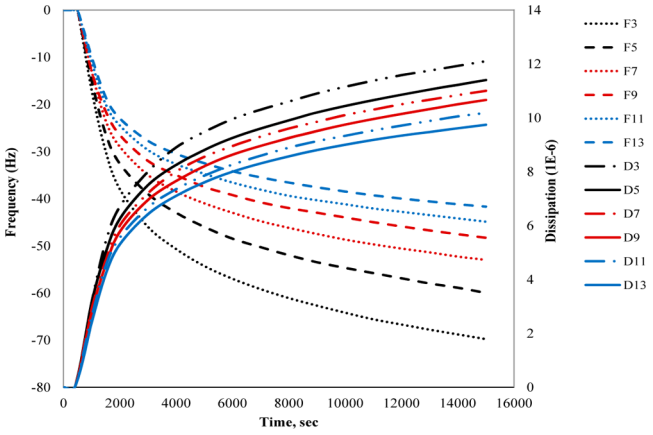

Figure 3. Frequency and dissipation changes versus time for the adsorption of *n*-C_5 asphaltene from the asphaltene + toluene system onto a gold quartz crystal surface.

Voinova et al. derived the general solution of a wave equation describing the dynamics of two-layer viscoelastic polymer materials of arbitrary thickness deposited on quartz surfaces in a fluid environment.[27] Within the Voigt model of a viscoelastic element, Voinova et al. calculated the acoustic response of the system to an applied shear stress.[27] The Voigt model assumptions are as follows: (1) a laterally homogeneous and evenly distributed film, (2) the bulk fluid being Newtonian, (3) the adsorbed layer coupling perfectly to the sensor (no slip), and (4) the observed signal only being due to the film.

The necessary input parameters for using the Voigt model are as follows: (1) Δf and ΔD from different overtones, (2) layer density, and (3) solvent density and viscosity (pure solvent without the solute used for adsorption).

The Voigt model, available in the QTools software from Q-Sense, is used in this study for viscoelastic modeling of frequency and dissipation changes. The mass adsorbed (amount/thickness and viscosity) thus obtained with time is treated as experimental data like all other QCM−D experiments in the literature.

3.2. Adsorbed Mass Modeling. In this paper the term "Deposition" is used in general for any process of asphaltene adhesion onto a solid surface. Before asphaltene precipitation onset, where all asphaltene are stable in the system, the term "Adsorption" may also be used. After precipitation onset, only the term "Deposition" is used throughout this paper.

A quantitative theory of kinetic−diffusive−convective adsorption in a flow cell was developed by Filippov for different adsorption isotherms.[28] The transient convective diffusion equation governing the transport of adsorbate molecules in the flow cell is given by

$$\frac{\partial c(x, y, t)}{\partial t} + V_x(y)\frac{\partial c(x, y, t)}{\partial x} = D\frac{\partial^2 c(x, y, t)}{\partial y^2} \quad (5)$$

where $c(x,y,t)$ is the adsorbate concentration in the flow cell, x is the coordinate in the direction of flow, y is the coordinate in the direction normal to the interface, D is the diffusion coefficient, and $V_x(y)$ is the axial linear velocity. Figure 4 shows the flow cell geometry.

For the velocity profile, we have

$$V_x(y) = \gamma y\left(1 - \frac{y}{b}\right) \quad (6)$$

where

$$\gamma = \frac{6Q}{b^2 d} \quad (7)$$

and γ is the wall shear rate, Q is the volumetric flow of solution through the rectangular flow channel, L is the length of the channel, and b and d are the thickness and width of the flow cell, respectively. For the current flow system (i.e., the sensor crystal inside the flow module), the crystal active diameter is 1.0 cm and its active surface is 0.785 cm^2. We consider L as 1.0 cm,

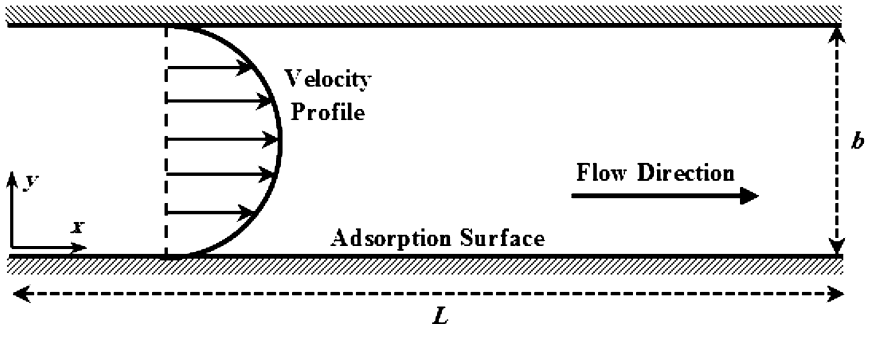

Figure 4. Flow cell geometry.

dx.doi.org/10.1021/ef401857t | *Energy Fuels* 2014, 28, 1617−1628

b as 2 mm, and to have the value of 0.785 cm^2 for the active surface, d should be 0.785 cm.

Equation 5 is to be solved for initial (eq 8) and boundary (eq 9) conditions. Equation 10 is to be solved for the adsorbed amount, and eq 11 is to be solved for the adsorption kinetics

$$\text{at } t = 0,\ c = 0 \text{ for all } y \text{ and } x > 0 \tag{8}$$

$$\text{at } x = 0,\ c = c_0 \text{ for all } y \text{ and } t \tag{9}$$

$$\Gamma(x, t) = \int_0^{b/2} \left[c\left(x, \frac{b}{2}, t\right) - c(x, y, t) \right] dy \tag{10}$$

$$\frac{\partial \Gamma(x, t)}{\partial t} = K_{ad}[c(x, 0, t)]^m [\Gamma_m^0 - \Gamma(x, t)]^r - K_{des}\Gamma(x, t) \tag{11}$$

where c_0 is the adsorbate concentration in the bulk, Γ_m^0 is the maximum adsorption, $c(x,0,t)$ is the surface concentration, m and r are the parameters of adsorption and desorption kinetics (for Henry adsorption kinetics, $m = 1$ and $r = 0$; for Langmuir adsorption kinetics, $m = r = 1$), and K_{ad} and K_{des} are the rate constants for adsorption and desorption, respectively. The adsorbed amount per unit surface, $\Gamma(x,t)$, is given by eq 10, where $[c(x,b/2,t) - c(x,0,t)]$ is the excess concentration in the adsorbed layer. Parameter b is the thickness of the flow channel. The concentration distribution in the flow channel, $c(x,y,t)$, is symmetrical with respect to the plane $(y = b/2)$, because the normal flux, $\partial c(x,b/2,t)/\partial y$, is equal to zero. Filippov showed that it is reasonable to consider asymptotic analytical solutions for initial and long times.

4. RESULTS AND DISCUSSION

In this paper, a solution of asphaltene in toluene or *n*-heptane + toluene (heptol) is used as the model oil system. A constant asphaltene concentration of 100 ppm is used for all of the experiments, because the effect of this parameter has been widely investigated by others.[13,14] Each experiment is repeated 3 times, and the average results are presented in this paper. As previously explained in the Modeling section, all experimental results showed a viscoelastic behavior of the adsorbed layer from the model oil system. Therefore, the Voigt model in the QTools software is applied for interpreting the mass adsorbed from frequency and dissipation changes.

4.1. Accuracy of Voigt Viscoelastic Modeling. To verify the accuracy of viscoelastic modeling results, AFM is applied to find the thickness of the adsorbed layer on the sensor crystal surface after the experiment. For the same experiment, Figures 5 and 6 show the QCM−D result for the thickness of the adsorbed asphaltene layer and AFM image for the asphaltene-deposited surface of the gold crystal, respectively. This QCM−D experiment was run with *n*-C_5 asphaltene in toluene at 80 °C and at a 80 μL/min flow rate. A comparison of Figures 5 and 6 shows that the viscoelastic modeling result is in reasonable agreement with the AFM result for the adsorbed layer thickness. Figure 7 represents the thickness analysis of the AFM image shown in Figure 6. It shows the percentage of each thickness in the total surface of the AFM image. According to Figure 7, more than 90% of the surface is covered with layers with a thickness of 20−40 nm. Also, the average thickness is 28.47 nm, which is very close to the result of the Voigt model shown in Figure 5.

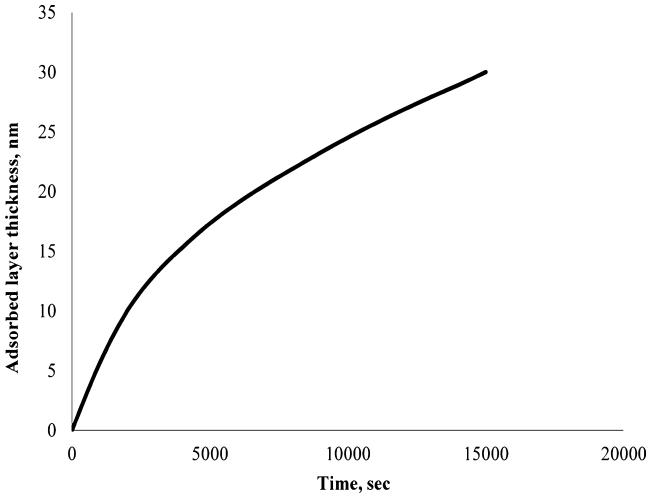

Figure 5. QCM−D Voigt model result for the thickness of the adsorbed layer from the *n*-C_5 asphaltene + toluene system onto a gold crystal surface versus time at 80 °C and at a 80 μL/min flow rate.

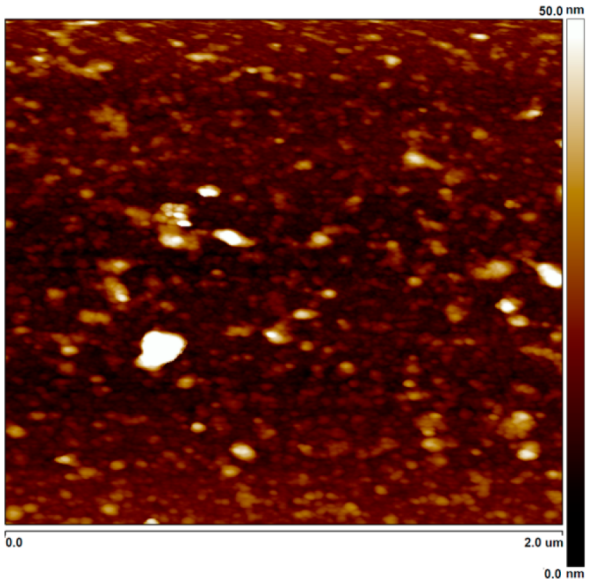

Figure 6. AFM image of the gold crystal surface after the QCM−D experiment using a *n*-C_5 asphaltene + toluene model oil system at 80 °C and at a 80 μL/min flow rate.

It can also be seen from Figure 6 that the adsorbed mass is distributed uniformly on the surface of the sensor crystal, except for a few locations. A high thickness at these few locations is because of the dust particles depositing on the gold crystal surface during the transfer of the sensor crystal from the QCM−D setup to the AFM apparatus.

4.2. Temperature. Figure 8 presents the effect of the temperature on the amount of adsorbed mass from *n*-C_5 asphaltene in toluene onto a gold crystal surface versus time at a constant flow rate of 80 μL/min. The asphaltene at all four temperatures is stable in the solution, and far away from the precipitation onset. It can be seen from Figure 8 that the maximum adsorbed mass after 4 h is increasing when the temperature increases from 20 to 80 °C. Because the concentration of asphaltene in the model oil used in this study is very low (100 ppm), viscosity of the model oil is very close to the viscosity of pure toluene. Table 1 represents

dx.doi.org/10.1021/ef401857t | Energy Fuels 2014, 28, 1617−1628

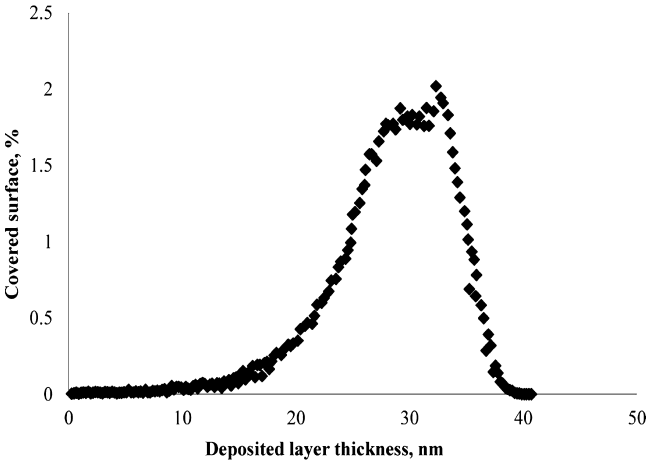

Figure 7. Thickness analysis of the AFM image shown in Figure 6

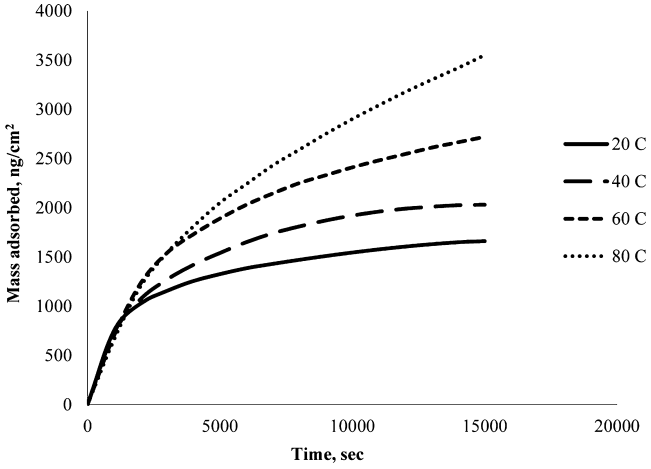

Figure 8. Effect of the temperature on the amount of adsorbed mass from the *n*-C_5 asphaltene + toluene system onto a gold crystal surface versus time at a 80 μL/min flow rate.

viscosity of pure toluene at different temperatures.[29] These values are used for viscoelastic modeling of frequency and dissipation changes in this work.

Table 1. Viscosity of Pure Toluene at Different Temperatures

temperature (°C)	toluene viscosity (cP)
20	0.586
40	0.460
60	0.371
80	0.307

As the temperature increases, the solution viscosity would decrease, and therefore, both the temperature increase and viscosity decrease will result in a higher diffusion coefficient for asphaltene particles in the model oil system. A higher diffusion coefficient will cause a higher amount for mass adsorbed, because the adsorption is mainly controlled by diffusion at long times, as discussed later in this subsection.

An interesting observation in Figure 8 is that, for the temperatures of 60 and 80 °C, the rate of increase in the adsorbed mass at long times is much more than the temperatures of 20 and 40 °C. In other words, it seems that, for the temperatures of 20 and 40 °C, the saturation plateaus will be observed sooner than 60 and 80 °C. Figure 9 shows the

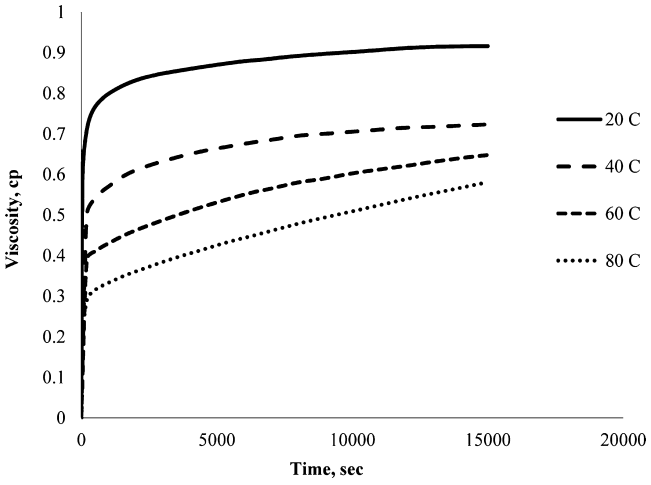

Figure 9. Effect of the temperature on the viscosity of adsorbed mass from the *n*-C_5 asphaltene + toluene system onto a gold crystal surface versus time at a 80 μL/min flow rate.

effect of the temperature on the viscosity of adsorbed mass from *n*-C_5 asphaltene in toluene onto a gold crystal surface versus time at a constant flow rate of 80 μL/min. As expected, the viscosity is decreasing when the temperature increases from 20 to 80 °C but is always less than 1 cP. The viscosity value is small because the adsorbed mass consists of asphaltene molecules and asphaltene nanoaggregates but not bulk asphaltene. Viscosity of the adsorbed layer at 60 and 80 °C does not reach an equilibrium value because the total mass adsorbed at 60 and 80 °C does not reach equilibrium within the experimental time scale of 4 h.

To model the amount of mass adsorbed, the model presented by Filippov is applied. As per the model, if the slope of adsorption versus time is a linear function of time for initial times, then the adsorption process is controlled by the adsorption kinetics (eqs 12a and 12b). If the mass adsorbed follows a linear relationship with the square root of time at a short stage of the experiment, then the rate of adsorption depends upon the diffusion coefficient, *D*, and does not depend upon parameters characterizing the kinetics and convective transfer (eqs 13a and 13b)

$$\Gamma(t) = St \tag{12a}$$

where

$$S = K_{ad} c_0^{\,m} (\Gamma_m^0)^r \tag{12b}$$

S is the slope and K_{ad} is the rate constant of adsorption

$$\Gamma(t) = St^{1/2} \tag{13a}$$

where

$$S = 2c_0 \left(\frac{D}{\pi}\right)^{1/2} \tag{13b}$$

For long times, Filippov showed that the adsorption process is governed by the diffusion as well as the convective transfer. He presented an analytical solution for the mass adsorbed versus time at long times and compared the relative mass adsorbed versus time for different adsorption isotherms.

dx.doi.org/10.1021/ef401857t | *Energy Fuels* 2014, 28, 1617−1628

In the current study, modeling results showed that, for initial time, the amount of mass adsorbed is a linear function of time, which means that the rate of adsorption depends upon K_{ad} and does not depend upon the parameters characterizing diffusion and convective transfer. Therefore, for this case, the adsorption process is controlled by adsorption kinetics. The adsorption process for long times is governed by diffusion and convective transfer. For both initial and long times, the Henry adsorption isotherm showed a reasonable match for the adsorption of n-C_5 asphaltene from the model oil system onto a gold crystal at different temperatures and at a constant flow rate of 80 μL/min. Figures 10, 11, 12, and 13 present initial and long time modeling results versus experimental mass adsorbed for temperatures of 20, 40, 60, and 80 °C, respectively.

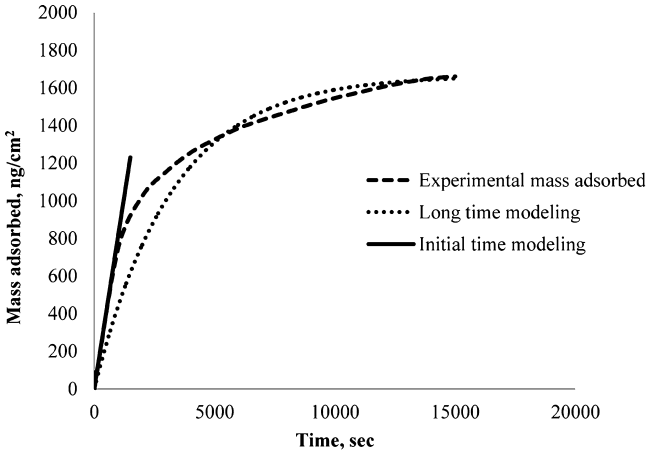

Figure 10. Experimental and modeling results for the amount of adsorbed mass from the n-C_5 asphaltene + toluene model oil onto a gold crystal surface versus time at 20 °C and at a 80 μL/min flow rate.

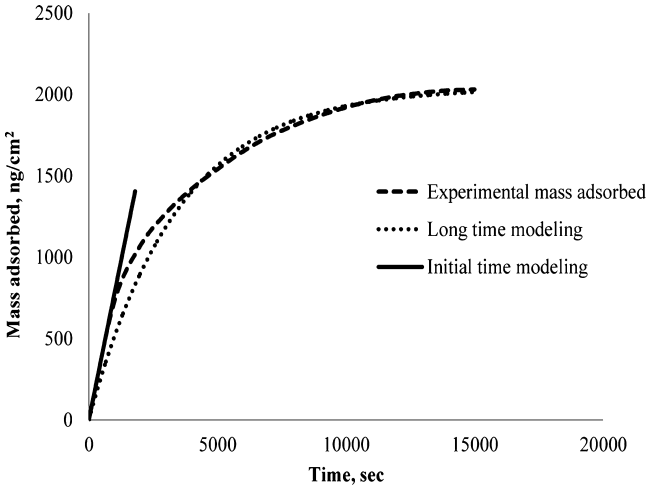

Figure 11. Experimental and modeling results for the amount of adsorbed mass from the n-C_5 asphaltene + toluene model oil onto a gold crystal surface versus time at 40 °C and at a 80 μL/min flow rate.

Table 2 presents the values of parameters used to match the experimental amount of adsorbed mass with time. For initial time, the rate constant of adsorption and, for a long time, the diffusion coefficient are used. For an initial time scale, the rate constant of adsorption is decreasing when the temperature increases, representing a lower amount of mass adsorbed at higher temperatures during initial stages of the experiment.

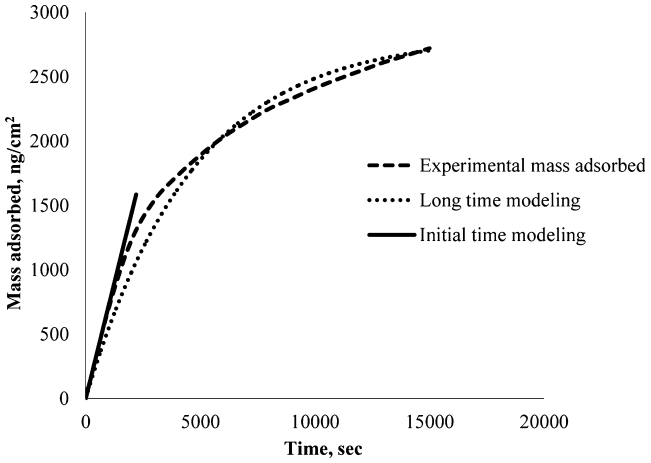

Figure 12. Experimental and modeling results for the amount of adsorbed mass from the n-C_5 asphaltene + toluene model oil onto a gold crystal surface versus time at 60 °C and at a 80 μL/min flow rate.

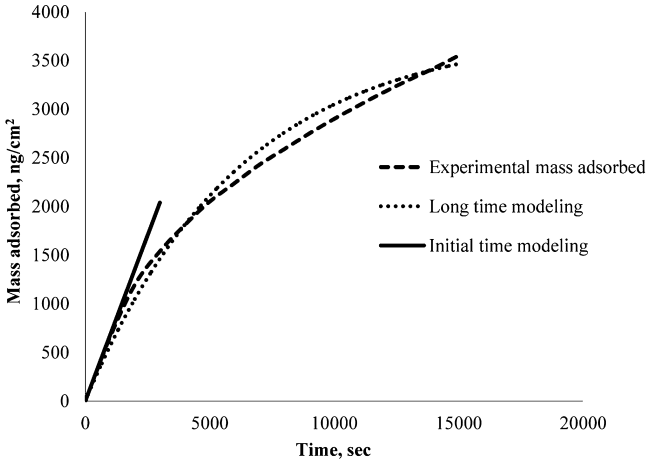

Figure 13. Experimental and modeling results for the amount of adsorbed mass from the n-C_5 asphaltene + toluene model oil onto a gold crystal surface versus time at 80 °C and at a 80 μL/min flow rate.

Table 2. Model Parameters for the Amount of Mass Adsorbed from the n-C_5 Asphaltene + Toluene Model Oil onto a Gold Crystal Surface at Various Temperatures and a 80 μL/min Flow Rate

temperature (°C)	K_{ad} (s^{-1})	D (m^2/s)
20	0.0082	5.5×10^{-11}
40	0.0078	6.5×10^{-11}
60	0.0072	7.0×10^{-11}
80	0.0068	7.2×10^{-11}

However, for long times, the diffusion coefficient is increasing with temperature, which results in more amount of adsorbed mass at higher temperatures for a long time.

The values presented in Table 2 are in accordance with the Stokes−Einstein equation for diffusion of spherical particles through a liquid with low Reynolds number. An increase of the temperature will result in an increase in the diffusion coefficient value of the particle. Also, a decrease of both viscosity and particle size will result in a higher value for the diffusion coefficient. We believe that the asphaltene particle size does not change appreciably with the temperature in our model oil system. This is because of only a small difference between

dx.doi.org/10.1021/ef401857t | Energy Fuels 2014, 28, 1617−1628

diffusivity coefficients at various temperatures. This change is because of changes in the temperature and viscosity, and changes in the particle size will cause a larger difference between the diffusion coefficients of the particle at different temperatures. Also, asphaltenes are stable in the model oil at all four temperatures to neglect aggregation.

We could not detect when the first layer of asphaltene forms on the surface of the sensor using the QCM equipment. Before this first layer, we have asphaltene−metal interactions, and after forming the first layer, we have asphaltene−asphaltene interactions. From the obtained results, one may conclude that, at the initial stage of the experiments, where the adsorption process is controlled by the adsorption kinetics, the asphaltene−metal interactions are dominant and, at a long time of experiments, the asphaltene−asphaltene interactions play the main role in the adsorption process.

4.3. Asphaltene Polydispersity. To investigate the effect of asphaltene polydispersity, model oil solutions with *n*-C_5 asphaltene and *n*-C_7 asphaltene, each at 100 ppm, are used for adsorption at a 80 μL/min flow rate onto a gold crystal at 20 °C. Figures 14 and 15 present the effect of asphaltene polydispersity on the amount of adsorbed mass and viscosity of the adsorbed layer, respectively, from the two model oil systems. From Figure 14, it is observed that the maximum amount of mass adsorbed at equilibrium for *n*-C_5 asphaltene is much more than *n*-C_7 asphaltene and the *n*-C_7 asphaltene mass adsorbed reaches equilibrium much sooner than *n*-C_5 asphaltene. This shows that the C_{5-7} asphaltene fraction plays an important role in the adsorption of asphaltene onto a gold crystal surface. From Figure 15, it can be observed that the adsorbed *n*-C_7 asphaltene viscosity is higher than *n*-C_5 asphaltene viscosity, which is in line with the fact that *n*-C_7 asphaltene are heavier with a higher molecular weight than *n*-C_5 asphaltene.

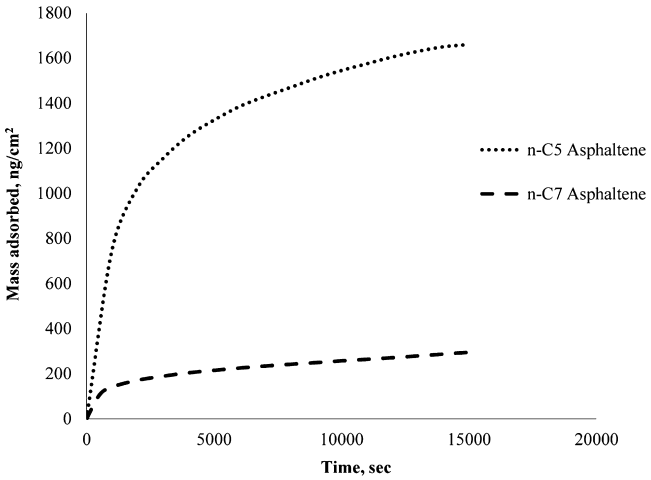

Figure 14. Amount of adsorbed mass from the model oil system onto a gold crystal surface versus time at 20 °C and at a 80 μL/min flow rate.

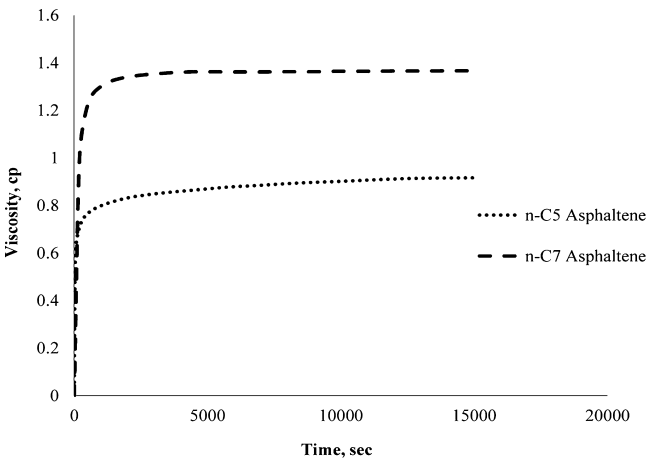

Figure 15. Viscosity of adsorbed mass from the model oil system onto a gold crystal surface versus time at 20 °C and at a 80 μL/min flow rate.

The C_{5-7} asphaltene subfraction has a higher diffusion rate because it is lighter with a lower molecular weight in comparison to the C_{7+} asphaltene subfraction, and this higher diffusion rate results in a higher mass adsorbed for *n*-C_5 asphaltene. The amount of the C_{5-7} asphaltene subfraction is high in *n*-C_5 asphaltene content of the crude oil used in this study. The *n*-C_5 asphaltene content of this crude oil is 2.8 wt %, and its *n*-C_7 asphaltene content is 1.1 wt %.

For the modeling of mass adsorbed with time, the same procedure used for *n*-C_5 asphaltene is applied for *n*-C_7 asphaltene. Modeling results showed that, at initial time, the amount of mass adsorbed is a linear function of time, which means that the rate of adsorption depends upon K_{ad} and does not depend upon the parameters characterizing diffusion and convective transfer. Therefore, for this case, the adsorption process is controlled by adsorption kinetics. The adsorption process for long times is governed by diffusion and convective transfer. For long times, the Langmuir adsorption isotherm is seen to find a reasonable match for the adsorption of *n*-C_7 asphaltene from the model oil system onto a gold crystal. This is because the Langmuir adsorption isotherm reaches equilibrium much sooner than the Henry isotherm. The same trend is observed in Figure 14 between *n*-C_5 asphaltene and *n*-C_7 asphaltene, where the *n*-C_7 asphaltene mass adsorbed reaches equilibrium much sooner than the *n*-C_5 asphaltene mass.

The rate constant of adsorption used to model the amount of mass adsorbed for *n*-C_7 asphaltene at initial times is 0.0022 per second. For long times, a diffusion coefficient of 2.7×10^{-11} is used. Figure 16 presents initial and long time modeling results versus experimental mass adsorbed at 20 °C. In Figure 16, experimental data and modeling results are not clear during initial times because of overlap. Hence, the results are magnified in Figure 17 for an initial time scale of the experiment.

It can be observed from Figure 17 that, during initial time, using the kinetics of adsorption shows a better match in comparison to the long-time modeling, which uses diffusion and convective transfer.

4.4. Solvent (Asphaltene Stability). To understand the effect of solvent on the amount of deposited mass, heptol model oil systems with a constant asphaltene concentration of 100 ppm are used. To find the onset of precipitation, the procedure described in the Asphaltene Precipitation Onset Measurement section is applied. Figure 18 presents the absorbance as a function of the heptane volume percent for an UV−vis wavelength of 500 nm and using toluene as the blank. The intersection of two straight lines that pass through the data points shows the volume percent of *n*-heptane at precipitation onset. For the model oil used in this study (100 ppm of *n*-C_7 asphaltene in heptol), the precipitation onset

dx.doi.org/10.1021/ef401857t | Energy Fuels 2014, 28, 1617−1628

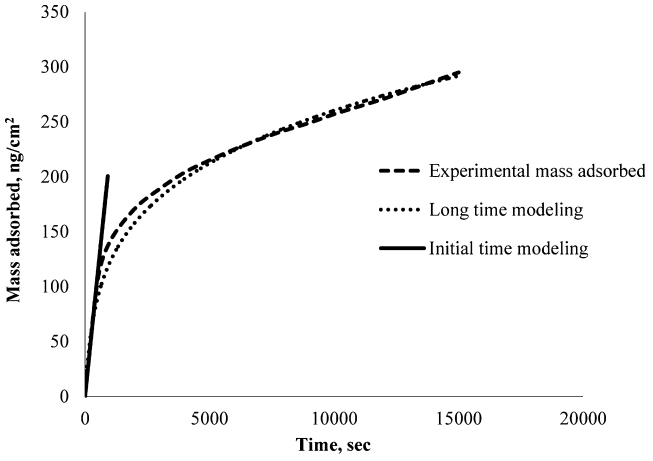

Figure 16. Experimental and modeling results for the amount of adsorbed mass from the *n*-C_7 asphaltene + toluene model oil onto a gold crystal surface versus time at 20 °C and at a 80 μL/min flow rate.

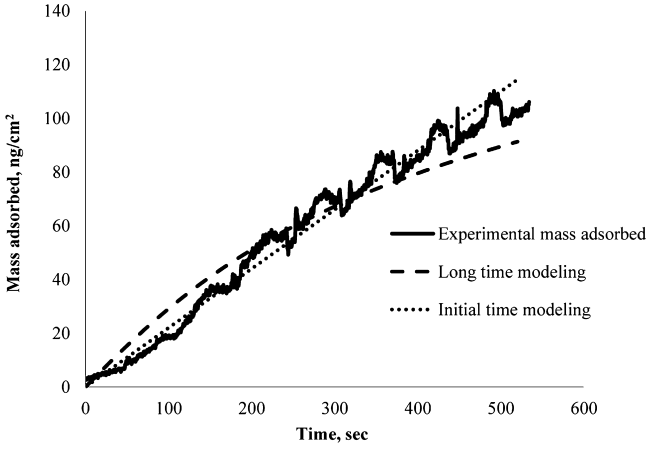

Figure 17. Comparison of experimental and modeling results for the amount of adsorbed mass from the *n*-C_7 asphaltene + toluene system onto a gold crystal surface at 20 °C during initial time. The flow rate is 80 μL/min.

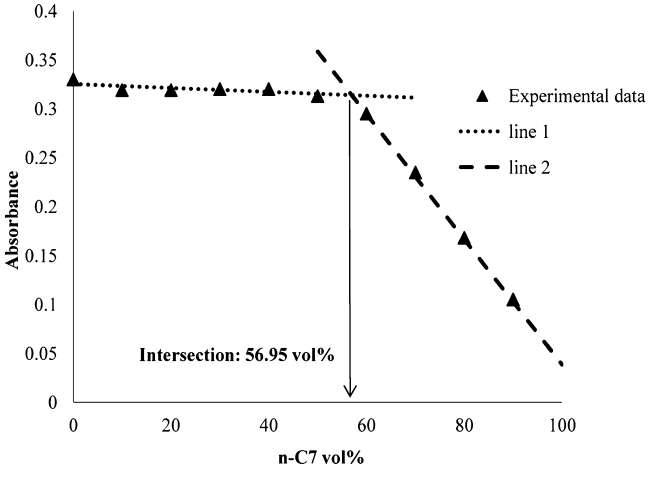

Figure 18. Precipitation onset measurement using an absorbance of UV−vis at 500 nm wavelength.

happens at 56.95 vol % *n*-heptane based on the results obtained from Figure 18.

It should be mentioned that using different UV−vis wavelengths produced almost the same result for the volume percent of *n*-heptane at the precipitation onset. Figures 19 and

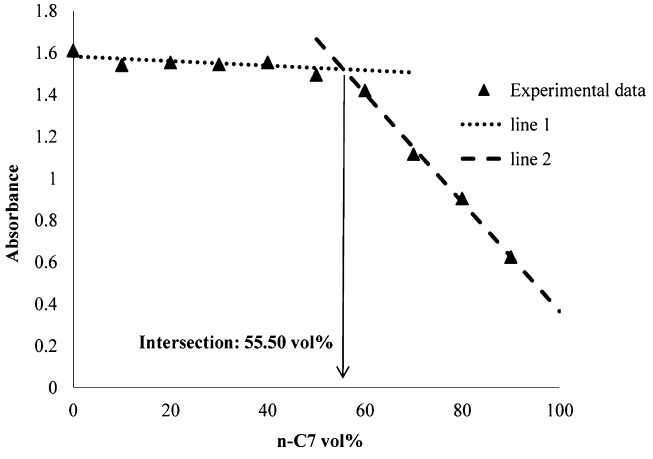

Figure 19. Precipitation onset measurement using an absorbance of UV−vis at 300 nm wavelength.

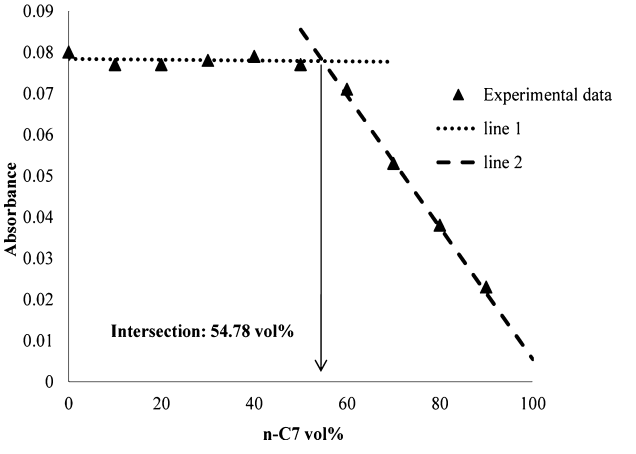

Figure 20. Precipitation onset measurement using an absorbance of UV−vis at 700 nm wavelength.

20 present the absorbance at UV−vis wavelengths of 300 and 700 nm, respectively, as a function of the heptane volume percent. On the basis of the results obtained from Figures 19 and 20, the precipitation onset happens at 55.50 and 54.78 vol % *n*-heptane, respectively, which are very close to the value obtained at an UV−vis wavelength of 500 nm.

Figure 21 shows the deposition of 100 ppm *n*-C_7 asphaltene from heptol solutions with different volume fractions of heptane and toluene. No saturation plateau is observed for heptol 50:50 and 75:25 within the experimental time scale.

On the basis of the experimental results, when the ratio of heptane/toluene increases, the amount of corresponding deposited mass increases up to a certain ratio and decreases beyond that. This maximum amount of asphaltene deposition is occurring for a heptol solution with equal amounts of heptane and toluene and is near the asphaltene precipitation onset for our model oil system. After precipitation onset, asphaltene aggregates, forming larger particles that can pass through the sensor crystal surface without depositing because of convective

dx.doi.org/10.1021/ef401857t | *Energy Fuels* 2014, 28, 1617−1628

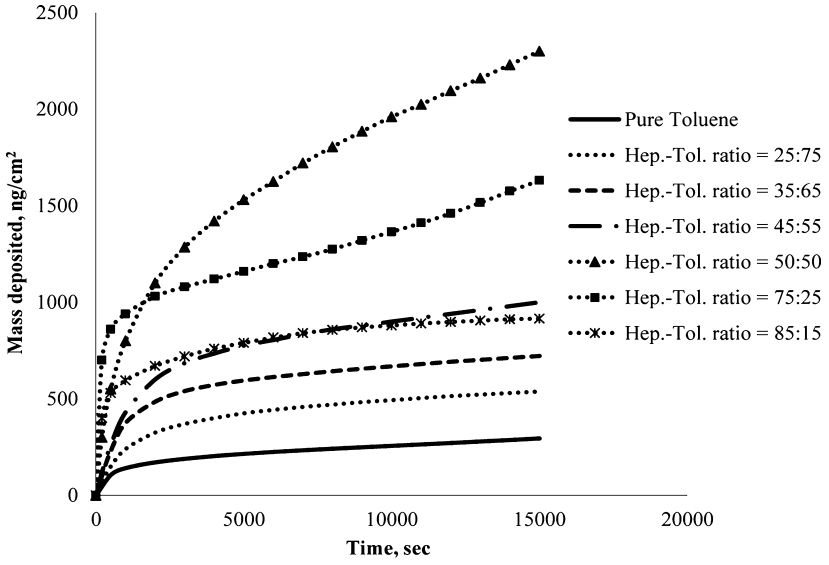

Figure 21. Effect of solvent on the amount of deposited mass from *n*-C_7 asphaltene + heptol systems onto a gold crystal surface versus time at 20 °C and at a 80 μL/min flow rate.

transfer. In other words, it is assumed that, beyond precipitation onset, only the asphaltene primary particles participate in the deposition process. The large aggregated particles because of inertia are considered to be carried out with the flow. Similar reasonable assumptions have been made in studies of other researchers in the area of modeling asphaltene deposition in pipelines.[30,31]

From Figure 21, it is observed that, after precipitation onset, the initial change in the deposited mass is faster, which shows the deposition of asphaltene primary particles and nano-aggregates beyond precipitation onset. These primary particles are larger than asphaltene molecules, which form the main part of the adsorbed layer before precipitation onset.

4.5. Depositing Surface. To investigate the interaction between asphaltene and pipeline material, carbon steel and iron oxide sensor crystals are used. Many pipelines used for crude oil transport are made of carbon steel. Iron oxide presents the case of rust and can provide an insight into the change in asphaltene deposition behavior because of a rusted pipeline compared to a new steel pipeline.

Figure 22 shows the amount of adsorbed mass from the *n*-C_5 asphaltene + toluene system onto gold, iron oxide, and carbon steel crystals versus time at 20 °C and at a 80 μL/min flow rate. It can be observed from Figure 22 that, when a steel pipeline is rusted, the mass adsorbed during initial stages increases but it shows a decrease in a long run. Both carbon steel and iron oxide surfaces represent more mass adsorbed in comparison to a gold surface.

4.6. Flow Rate. QCM−D experiments are performed at various flow rates to check the effect of convective transfer on the asphaltene adsorption process. The results are plotted in Figure 23. It can be observed from Figure 23 that the rate of adsorption is nearly independent of the flow rates during initial time scale. However, after a long time, the effect of the flow rate is significant. The near independence of initial asphaltene adsorption on the flow rates shows a negligible effect of convective transfer on the adsorption process.

At long times, an increase of the flow rate causes more mass adsorbed on the sensor crystal. An increase in the flow rate increases the wall shear rate, which is against the particle

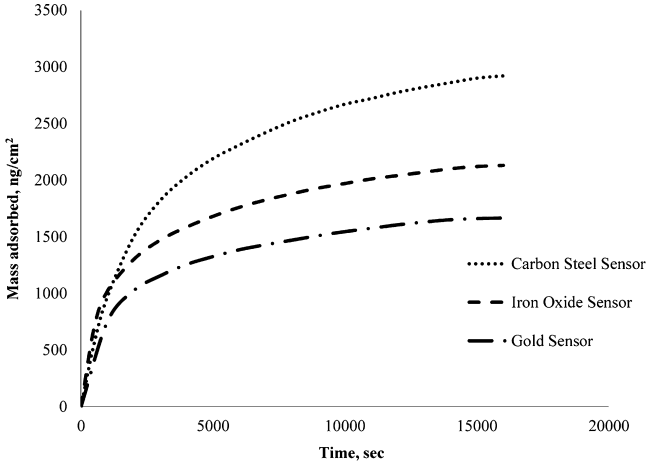

Figure 22. Adsorbed mass amount from the *n*-C_5 asphaltene + toluene system onto different surfaces versus time at 20 °C and at a 80 μL/min flow rate.

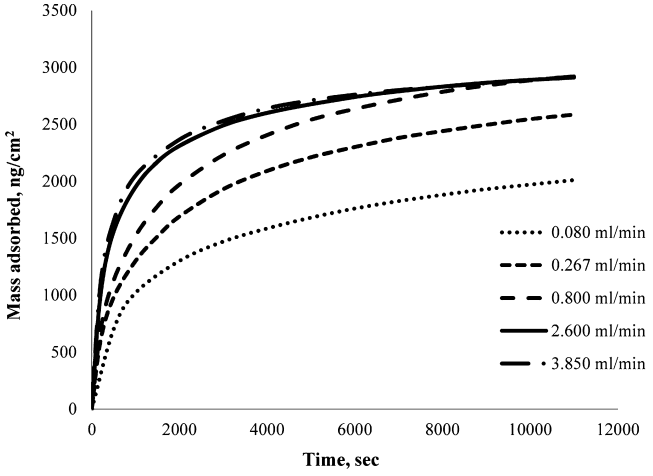

Figure 23. Effect of the flow rate on the amount of adsorbed mass from the *n*-C_5 asphaltene + toluene system onto an iron oxide crystal surface versus time at 20 °C and at different flow rates.

dx.doi.org/10.1021/ef401857t | *Energy Fuels* 2014, 28, 1617−1628

deposition on the sensor crystal. However, at the same time, the sensor crystal is provided with more amount of asphaltene, and the net result of these two effects causes more mass adsorbed on the sensor crystal. In a wellbore/pipeline with a high concentration of asphaltene in the bulk, the deposition is not limited by the availability of asphaltene and only the effect of the shear rate is dominant with changes in the flow rate. In such cases, an increase in the flow rate will decrease the amount of asphaltene deposited. In this study, all experiments with different flow rates are in the laminar region. For the maximum flow rate used (3.85 ml/min), both Reynolds number and shear rate are very small and in the order of 10^{-3} and 10^{-5} per second respectively.

Observed from Figure 23, at higher flow rates, the adsorption curve reaches equilibrium sooner than at lower flow rates. At very long times and at high enough flow rates, the rate of adsorption is independent of the flow rate. At very high flow rates (flow rates higher than 2.6 mL/min), the adsorption curves almost overlap, which means that there is no dependency to the flow rate for all times, from very short to very long.

5. CONCLUSION

In this paper, QCM−D experiments are performed to study different depositional aspects of asphaltene from model oil systems. The frequency and dissipation changes because of the adsorbed asphaltene layer showed a viscoelastic behavior of the deposit. The accuracy of QCM−D interpretation of adsorbed mass is ensured by comparing to the AFM result for an adsorbed asphaltene layer thickness. From the study presented in this paper, the following conclusions can be drawn for the model oil system by varying the depositing environment: (1) The adsorption process of n-C_5 asphaltene is controlled by adsorption kinetics during the initial stages of the experiment. The adsorption process at a long time is governed by diffusion and convective transfer. For both initial and long times, the Henry adsorption isotherm showed a reasonable agreement for the adsorption of n-C_5 asphaltene from the model oil system onto a gold sensor. (2) For initial times, the rate constant of adsorption is decreasing when the temperature increases, which correspond to a lower amount of mass adsorbed at higher temperatures for the initial time scale. However, for long times, the diffusion coefficient is increasing with the temperature, which results in more amount of adsorbed mass at higher temperatures in the long run. (3) Viscosity of the adsorbed layer decreases with an increase in the temperature. The viscosity value is small because the adsorbed mass consists of asphaltene molecules and not bulk asphaltene. (4) Polydispersity of asphaltene plays an important role in the deposition of asphaltene onto a gold surface. n-C_7 asphaltene mass adsorbed reaches equilibrium much sooner than n-C_5 asphaltene, and the maximum amount of mass adsorbed at equilibrium for n-C_5 asphaltene is much more than n-C_7 asphaltene. (5) Viscosity of the n-C_7 asphaltene deposit is higher than the viscosity of the n-C_5 asphaltene deposit because of the heavier nature of n-C_7 asphaltene compared to n-C_5 asphaltene. (6) The Langmuir adsorption isotherm is found to have a reasonable match for the adsorption of n-C_7 asphaltene from the model oil system onto a gold sensor crystal. (7) When the ratio of heptane/toluene increases, the amount of asphaltene mass deposited from the corresponding heptol solution increases up to the precipitation onset and decreases beyond that. After precipitation onset, asphaltene aggregates, forming larger particles that can pass through the sensor crystal surface without deposition because of convective transfer. (8) Investigation of different surface types showed that, when steel is rusted, the asphaltene mass adsorbed during initial time increases but, in a long run, shows a decrease. (9) Different flow rates demonstrated that the rate of adsorption is independent of the flow rate at initial time scale. However, for long times, the effect of the flow rate is significant. (10) The asphaltene adsorption curve reaches equilibrium sooner at higher flow rates. At very long times and at high enough flow rates, the rate of adsorption is independent of the flow rate. (11) At very high flow rates, the asphaltene adsorption curves have no dependency upon the flow rate and overlap for all times.

AUTHOR INFORMATION

Corresponding Author

*Telephone: 001-713-348-4900. E-mail: wgchap@rice.edu.

Author Contributions

†Mohammad Tavakkoli and Sai R. Panuganti contributed equally to this work.

Notes

The authors declare no competing financial interest.

ACKNOWLEDGMENTS

This work was undertaken with the funding from DeepStar and R&D Oil Subcommittee of Abu Dhabi National Oil Company. The authors are also thankful to Matthew Dixon, Mark Poggi, Jianxin Wang, Qilin Li, Lisa Biswal, Maura Puerto, and Clarence Miller for experimental suggestions, lab space, access to equipment, and helpful discussions.

NOMENCLATURE

f_0 = fundamental resonant frequency
n = overtone number
Δm = adsorbed mass
$\Delta\Gamma$ = adsorbed mass density
A = active area
ρ = density
ν = shear wave velocity
μ = shear modulus
h = thickness
C = constant
η = viscosity
Δf = change in frequency
ΔD = change in energy dissipation
c = adsorbate concentration
D = diffusion coefficient
x = coordinate in the direction of flow
y = coordinate in the direction normal to flow
t = time
V = velocity
γ = wall shear rate
Q = volumetric flow rate
L = length of the channel
b = thickness of the flow cell
d = width of the flow cell
c_0 = adsorbate concentration in the bulk
Γ_m^0 = maximum adsorption
m = parameter of adsorption kinetics
r = parameter of desorption kinetics
K = rate constant

Subscripts

q = quartz
l = liquid
s = solvent
x = coordinate in the direction of flow
y = coordinate in the direction normal to flow
ad = adsorption
des = desorption

REFERENCES

(1) Al-Maamari, R. S. H.; Buckley, J. S. *SPE Reservoir Eval. Eng.* **2003**, *6*, 210−214.
(2) Creek, J. L. *Energy Fuels* **2005**, *19*, 1212−1224.
(3) Trimm, D. L. Catalysts in petroleum refining and petrochemical industries. *Studies in Surface Science and Catalysis*; Elsevier Science B.V.: Amsterdam, Netherlands, 1996; Vol. *100*, pp 65−76.
(4) Qu, X.; Alvarez, P. J. J.; Li, Q. *Environ. Sci. Technol.* **2012**, *46*, 13455−13462.
(5) Baradel, N.; Fort, S.; Halila, S.; Badi, N.; Lutz, J. F. *Angew. Chem.* **2013**, *52*, 2335−2339.
(6) Moya, S. E.; Irigoyen, J. *J. Polym. Sci., Part B: Polym. Phys.* **2013**, *51*, 1068−1072.
(7) Frost, R.; Svedhem, S. *Cell. Subcell. Nanotechnol. Methods Mol. Biol.* **2013**, *991*, 127−137.
(8) Nam, D. H.; Lee, J. O.; Sang, B. I.; Won, K.; Kim, Y. H. *Appl. Biochem. Biotechnol.* **2013**, *170*, 25−31.
(9) Ozdemir, M. S.; Marczak, M.; Bohets, H.; Bonroy, K.; Roymans, D.; Stuyver, L.; Vanhoutte, K.; Pawlak, M.; Bakker, E. *Anal. Chem.* **2013**, *85*, 4770−4776.
(10) Lin, S.; Wiesner, M. R. *Environ. Sci. Technol.* **2012**, *46*, 13270−13277.
(11) Gall, I.; Herzberg, M. H.; Oren, Y. *Soft Matter* **2013**, *9*, 2443−2452.
(12) Salas, C.; Rojas, O. J.; Lucia, L. A.; Hubbe, M. A.; Genzer, J. *Appl. Mater. Interfaces* **2013**, *5*, 199−206.
(13) Ekholm, P.; Blomberg, E.; Claesson, P.; Auflem, I. H.; Sjoblom, J.; Kornfeldt, A. *J. Colloid Interface Sci.* **2002**, *247*, 342−350.
(14) Xie, K.; Karan, K. *Energy Fuels* **2005**, *19*, 1252−1260.
(15) Rudrake, A.; Karan, K.; Horton, J. H. *J. Colloid Interface Sci.* **2009**, *332*, 22−31.
(16) Farooq, U.; Sjoblom, J.; Øye, G. *J. Dispersion Sci. Technol.* **2011**, *32*, 1388−1395.
(17) Vargas, F. M. *Proceedings of the ADNOC Research and Development Academic Conference*; Abu Dhabi, United Arab Emirates, Feb 26−28, 2013.
(18) Abudu, A.; Goual, L. *Energy Fuels* **2009**, *23*, 1237−1248.
(19) Vargas, F. M. *Energy Fuels* **2013**, manuscript under preparation.
(20) Sauerbrey, G. *Z. Phys.* **1959**, *155*, 206−222.
(21) Kanazawa, K. K.; Gordon, J. G., II. *Anal. Chim. Acta* **1985**, *175*, 99−105.
(22) Kanazawa, K. K.; Gordon, J. G., II. *Anal. Chem.* **1985**, *57*, 1770−1771.
(23) Rodahl, M.; Kasemo, B. *Sens. Actuators, A* **1996**, *54*, 448−456.
(24) Andersson, F. *Q-Sense Webinar*, Dec 10, 2012.
(25) Martin, S. J.; Granstaff, V. E.; Frye, G. C. *Anal. Chem.* **1991**, *63*, 2272−2281.
(26) Cho, N. J.; D′Amour, J. N.; Stalgren, J.; Knoll, W.; Kanazawa, K.; Frank, C. W. *J. Colloid Interface Sci.* **2007**, *315*, 248−254.
(27) Voinova, M. V.; Rodahl, M.; Jonson, M.; Kasemo, B. *Phys. Scr.* **1999**, *59*, 391−396.
(28) Filippov, L. K. *J. Colloid Interface Sci.* **1995**, *174*, 32−39.
(29) Chemical Engineering Research Information Center (CHERIC). *Pure Component Database (Queriable Database)*; CHERIC: Seoul, South Korea (accessed May 12, 2007).
(30) Eskin, D.; Ratulowski, J.; Akbarzadeh, K.; Pan, S.; Lindvig, T. Modeling asphaltene deposition in oil transport pipelines. *Proceedings of the 7th International Conference on Multiphase Flow (ICMF)*; Tampa, FL, May 30−June 4th, 2010.
(31) Kurup, A. S.; Wang, J.; Subramani, H. J.; Buckley, J. S.; Creek, J. L.; Chapman, W. G. *Energy Fuels* **2012**, *26*, 5702−5710.